Journal of Alloys and Compounds 513 (2012) 518–523

Contents lists available at SciVerse ScienceDirect

Journal of Alloys and Compounds

journal homepage: www.elsevier.com/locate/jallcom

The microstructure and mechanical properties of deposited-IN718 by selective laser melting

Zemin Wang[a], Kai Guan[a], Ming Gao[a], Xiangyou Li[a,*], Xiaofeng Chen[b], Xiaoyan Zeng[a]

[a] Wuhan National Laboratory for Optoelectronics, School of Optoelectronics Science & Engineering, Huazhong University of Science & Technology, Wuhan 430074, PR China
[b] Research and Development Office of HUST, Huazhong University of Science & Technology, Wuhan 430074, PR China

ARTICLE INFO

Article history:
Received 14 September 2011
Received in revised form 17 October 2011
Accepted 29 October 2011
Available online 9 November 2011

Keywords:
Selective laser melting
Inconel 718
Microstructure
Mechanical property

ABSTRACT

Selective laser melting (SLM) technology based on powder bed has been used to manufacture IN718 samples. The starting material, manufacturing processes, heat treatment and characterization procedures of mechanical properties are presented. It is found that the microstructure is crucial for the mechanical properties of IN718. A regular microstructure with good metallurgical bonding, minimal defects and fine dendritic grains is formed by SLM. After heat treatment, the regular dendritic structure disappears and a needle-like δ phase precipitates at grain boundaries when γ′ and γ″ phases dissolve in the matrix. The microhardness of all samples shows directional independent. The tensile strengths and ductility of SLM + HTed IN718 at room temperature are comparative with those of the wrought IN718.

1. Introduction

IN718 is a solid solution or precipitation-hardenable nickel–chromium alloy containing significant amounts of iron, niobium, and molybdenum along with lesser amounts of aluminum and titanium. It has been widely used in gas turbine disks, rocket motors, spacecraft, nuclear reactors, pumps and tooling [1–3], due to its excellent hot corrosion resistance, fatigue resistance, wear resistance and good weldability with outstanding high strengths at elevated temperatures. However, it is difficult to manufacture the IN718 material by conventional machining methods at room temperature due to excessive tool wear and low material removal rates [4,5]. On the other hand, the applied IN718 components are very complex in shape with mazy inner chambers or overhangs and difficult to manufacture by a single conventional method. Current hybrid manufacturing methods with high cost and low efficiency is a good way to solve the above problem [6,7]. However, the known shortcomings, such as high rejection rate, material wastage, long lead-time and environmental impacts still cannot meet the requirement of wide applications.

Selective laser melting (SLM) is an additive layer-manufacturing process that uses 3D CAD (Computer Aided Design) data as a digital source, which provides an almost unchallenged freedom of design without the need for part-specific tooling [8–10]. It produces dense metal parts direct from the CAD using industry standard STL (Stereo Lithography) file format without any aid of tools and moulds. During fabrication, layers of fine metal powders are deposited by a powder bed and a high power laser fully melts the powder together to form the finished part based on the principle of rapid prototyping and laser cladding. With the aid of additive support structures and unirradiated powder, SLM technology has the capability to build any complex shape of metal parts that would otherwise be difficult or impossible to produce using conventional manufacturing processes [11]. Furthermore, SLM technology can greatly reduce the lead-time and investment cost for modules and dies design, hard or rare metal components fabrication, etc. [12].

In industry, some companies such as EOS and Inno-shape in Germany have built IN718 components successfully using SLM technology, which demonstrates that complex IN718 parts manufactured by SLM are promising to be applied in space and aviation area if mechanical properties meet the requirement. As we all know, the mechanical properties of IN718 are sensitive to microstructure that is dependent on the manufacturing methods. Thus far, no report on the manufacturing parameters and microstructure characterization of IN718 by SLM technology has been presented. The purpose of this investigation is to examine the formation ability of IN718 by SLM and compare its mechanical and microstructural characteristics to wrought product.

2. Experimental details

A self-developed SLM machine (LSNF-I) was used to process the IN718 powder. The self-developed SLM machine mainly consisted of a continuous wave IPG YLR-200 fiber laser (λ = 1.07 μm, maximum output power of 200 W, 100 μm spot size), an automatic powder delivery system, a building platform, and a computer system

* Corresponding author.
E-mail address: xyli@mail.hust.edu.cn (X. Li).

0925-8388/$ – see front matter © 2011 Elsevier B.V. All rights reserved.
doi:10.1016/j.jallcom.2011.10.107

Table 1
The chemical composition of IN718 super alloy powder.

Element	C	Cr	Mo	Al	Ti	Fe	Nb	Ni
Wt%	0.025	18.2	3.1	0.29	0.9	18.9	5.1	Balance

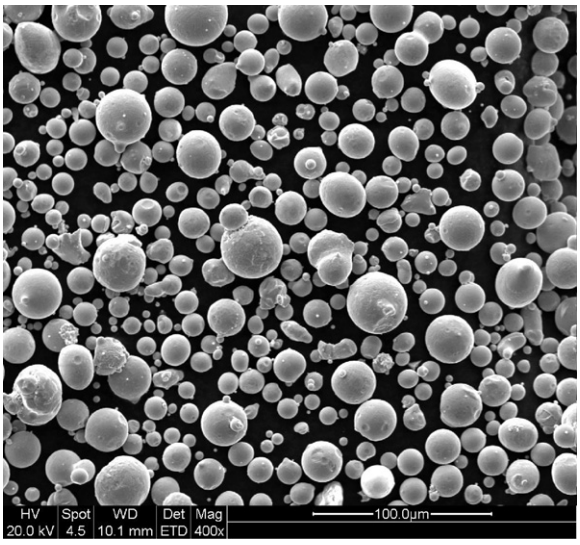

Fig. 1. SEM image showing characteristic morphology of IN718 powders.

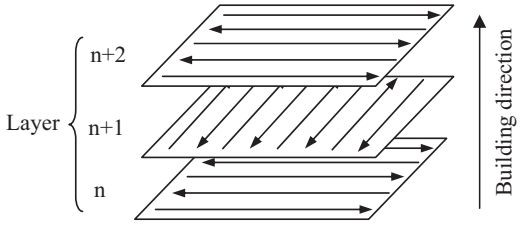

Fig. 2. Laser scanning strategy used in SLM experiments.

for process control. Special developed in-house software has two functions: one is slicing the 3D model of the part and producing laser scanning patterns to melt the metal powder layer selectively, the other is controlling the movements of the scanner, recoater, powder dispenser and building platform. The processes of SLM include: (i) a thin layer of metal powder is deposited by the recoater; (ii) the metal powder layer is melted by the incident laser beam to bond with the already solidified areas of the part underneath; (iii) the building platform is lowered by one layer thickness for the next powder deposition and laser exposure. With the repeat of above actions, the full part can be built layer by layer until the required shape is obtained. All the SLM experiments were conducted in an argon environment with O_2 concentration controlled below 40 ppm.

Gas atomized IN718 powders with a particle size below 50 μm were used as the starting material in SLM experiments, whose chemical composition is listed in Table 1. The morphology of the IN718 powders is shown in Fig. 1. All the raw samples were fabricated horizontally with their length direction paralleling with the surface of the substrate. During fabrication by SLM, a standard alternating *x*/*y*-raster strategy was chosen. This strategy features bidirectional hatches of a layer '*n*' performed in *x*-direction whilst the next layer '*n* + 1' turned 90°, as shown in Fig. 2. The SLM parameters used in this study are presented in Table 2. The as-fabricated samples were heat treated with the following schedule: solution treatment (980 °C, 1 h, air cooling) followed by double aging (720 °C, 8 h, furnace cooling + 620 °C, 8 h, air cooling).

Table 2
SLM manufacturing parameters used in this study.

Manufacturing parameters	Value
Laser power *P*, W	170
Laser scanning speed *V*, m/min	25
Overlap rate *O*, %	30
Powder layer thickness *δ*, μm	20

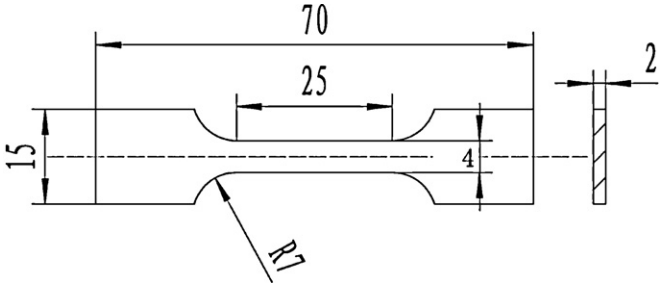

Fig. 3. Configuration of tensile testpieces used in this study.

Tensile testpieces were designed according to Chinese GB/T 228-2002 standard, as shown in Fig. 3. Two series of standard IN718 tensile testpieces of as-deposited and heat-treated were machined and examined using a zwick/roell tester to evaluate the tensile properties at room temperature (RT), respectively. For each series, three samples were included. Following testing, fracture faces of the tensile samples were characterized by a FEI Quanta 200 scanning electron microscopy (SEM). The chemical compositions were examined by energy dispersive spectroscopy (EDS) technique. Standard metallographic techniques and an optical microscopy (EPIPHOT 300) were used with the samples being etched with aqua regia for the materials. Vickers hardness tests on cross and vertical sections of samples were also carried out with a HVS-1000 microhardness tester at a load of 100 g to evaluate the uniformity of the microstructure.

3. Results and discussion

3.1. Microstructures

3.1.1. As-deposited by SLM

In our experiments, the density of the SLMed samples was determined using the 'Archimedes-method' in deionized water. The results show that all the SLMed samples are full solid with a relative density of nearly 100%.

Fig. 4 gives the optical micrographs of the fabricated IN718 samples by SLM. Under observations at lower magnifications by the optical microscope, the SLM formation features of line by line then layer by layer are shown clearly. Regular laser melted tracks corresponding to the alternating *x*/*y*-raster filling strategy are obtained on the cross section, as shown in Fig. 4(a). In Fig. 4(b), the cut ends of melted tracks could be seen in the form of a series of arcs induced by the Gauss energy distribution of laser. Obviously, all the ends of melted tracks are close stacked to form a good metallurgical bonding between two neighbor layers. Similar structures have been noted in SLM fabrication of 316L and Inconel 625 by other researchers [13,14]. Furthermore, SEM photos of two sections were generated to investigate the microstructure at a higher magnification, as shown in Fig. 5(a) and (b). A fine dendritic cast structure is formed, indicative of a very high cooling rate induced by high laser energy density. On the other hand, the grains are much smaller than those obtained by other laser processing technologies, such as direct laser fabrication technology based on blowing metal powder [15,16], which should be ascribed to the micron-size melting pool because the laser spot size is very small and the layer thickness is only 20 microns. On the cross section, the dendritic structure is littery due to the interplay of melted tracks under the raster filling strategy. In contrast, the regular solidification microstructure on the vertical section is clear, which is composed of parallel dendrites whose growing direction nearly parallels to *Z*-direction. In the process of cooling solidification of the liquid metal, due to the cooling effect caused by the substrate, heat mostly dissipates in the negative *Z*-direction. Under the action of the highest temperature gradient and solidification rate in the *Z*-direction, grains grow with the directional selection to form the dendrites. Finally, it is worth noting that some micropores are observed on both sections under high magnifications, as pointed by arrows in Fig. 5(a) and (b). These

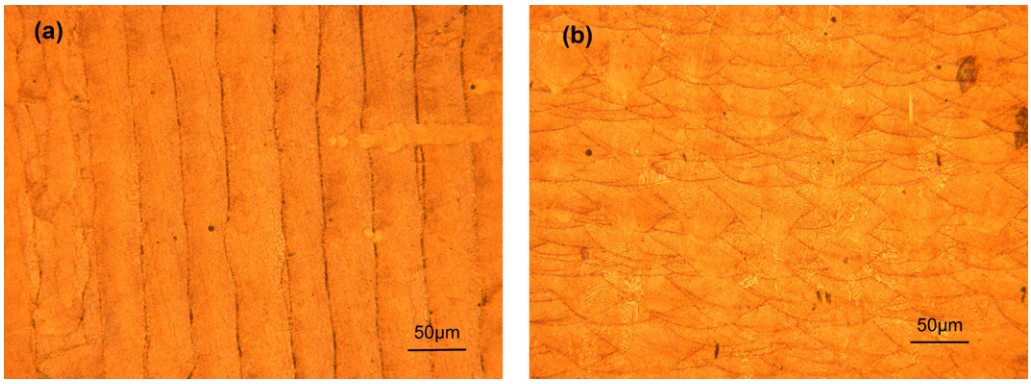

Fig. 4. Optical micrographs of SLMed IN718 samples on cross section (a) and vertical section (b).

micropores may influence the mechanical properties of the SLMed samples.

3.1.2. SLM plus heat treatment

Fig. 6 shows the microstructure of the SLMed samples after heat treatment. It is apparent that the regular dendritic crystals on both sections are demolished due to reheating, diffusion and recrystallization. A group of curved grain boundaries are developed. In Fig. 6(b), the long and narrow grains are still clearly shown to indicate the building direction of the sample. Meanwhile, there are numerous precipitates along grain boundaries on both sections. The EDS analysis for the precipitate (P1 in Fig. 6(b)) and matrix (P2 in Fig. 6(b)) are shown in Fig. 7. The O peak shown in Fig. 7(a) and (b) may be ascribed to the oxidization of metallurgical sample surface during corrosion. The results show that the precipitated structure is rich in Nb (19.1 in at.%) and Mo (10.23 in at.%) element, as shown in Fig. 7 (a). In contrast, as shown in Fig. 7(b), the contents of elements in the γ (face centered cubic) matrix are close to the chemical compositions presented in Table 1 when the measurement deviation is considered.

According to the EDS analysis, the niobium-rich precipitated structures at grain boundaries shown in Fig. 6(b) should be needle-like δ phase (rhombic crystal structure, stoichiometric composition as Ni_3Nb) and Laves phase (an embrittling TCP phase, such as (Ti, Nb)C type carbides). This result is similar as that observed by other researchers [17,18]. Generally, solidification in IN718 starts with a primary liquid → γ_reaction, and proceeds to cause enrichment of interdendritic liquid in Nb, Mo, Ti, C, etc., until an eutectic type reaction L → (γ + Laves) occurs to terminate the solidification process [19,20]. Due to the high cooling rate caused by SLM and the small content of Nb caused by the occurrence of abundant Laves phase, δ-phase cannot be precipitated during the process of SLM. During heat treatment, Laves phase is rather difficult to dissolve because of the poor diffusivity of large Nb atoms. However, in the present study, solution treatment at 980 °C is favorable for much of the Laves phase dissolving in the matrix. Thus, more Nb atoms are released around the Laves particles. On the other hand, the peak temperature of δ phase precipitation in IN718 is about 900 °C [21]. In solution treatment at 980 °C, needle-like δ phase precipitation occurs at grain boundaries when γ′ (cubic $L1_2$ crystal structure, stoichiometric composition as $Ni_3(Al, Ti)$) and γ″ (tetragonal $D0_{22}$ crystal structure, stoichiometric composition as Ni_3Nb) phases dissolve in the matrix. In the process of double aging treatment, γ′ and γ″ phases disperse and precipitate further in matrix to strengthen the alloy. In this work, the Laves phase dissolves incompletely because the solution temperature is still not high enough. Thus needle-like δ phase and Laves phase are found at grain boundaries, as shown in Fig. 6(b). γ′ and γ″ particles cannot be observed in SEM pictures because their size is generally less than 20 nm [22].

3.2. Mechanical properties

3.2.1. Microhardness

As a first indication for the uniformity of mechanical properties, microhardness is an important concern for the samples fabricated by SLM due to the additive manufacturing manner. Figs. 8 and 9 show the microhardness in the directions of *x*, *y* and 45° on two sections for SLMed and SLM + HTed (heat

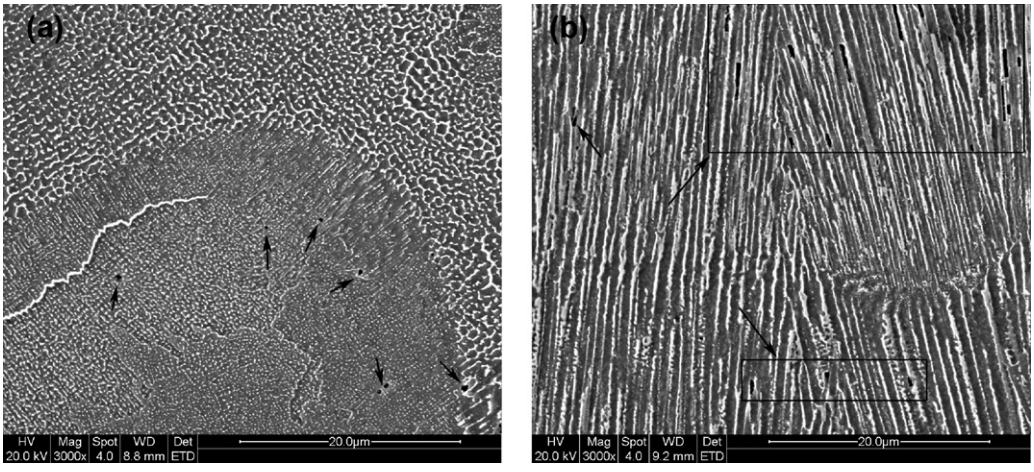

Fig. 5. SEM micrographs of SLMed IN718 samples on cross section (a) and vertical section (b).

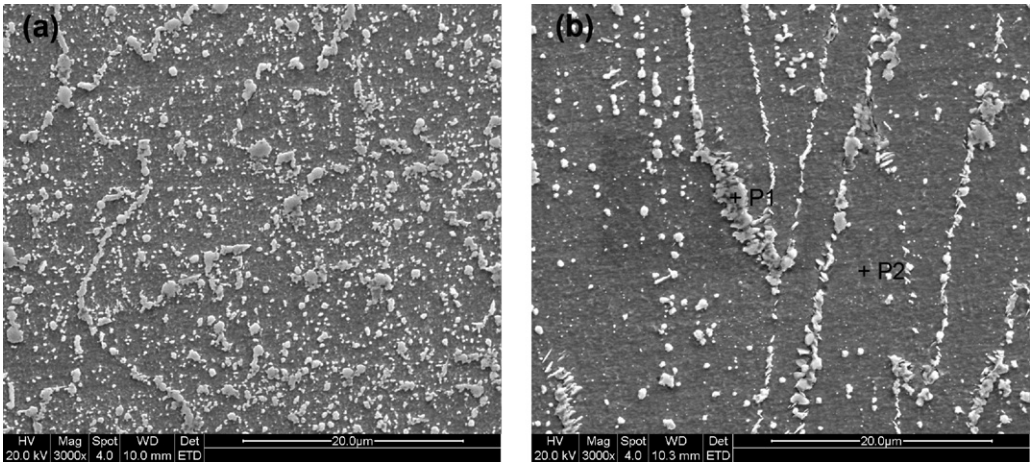

Fig. 6. SEM micrographs of SLM + heat treated (HTed) IN718 samples on cross section (a) and vertical section (b).

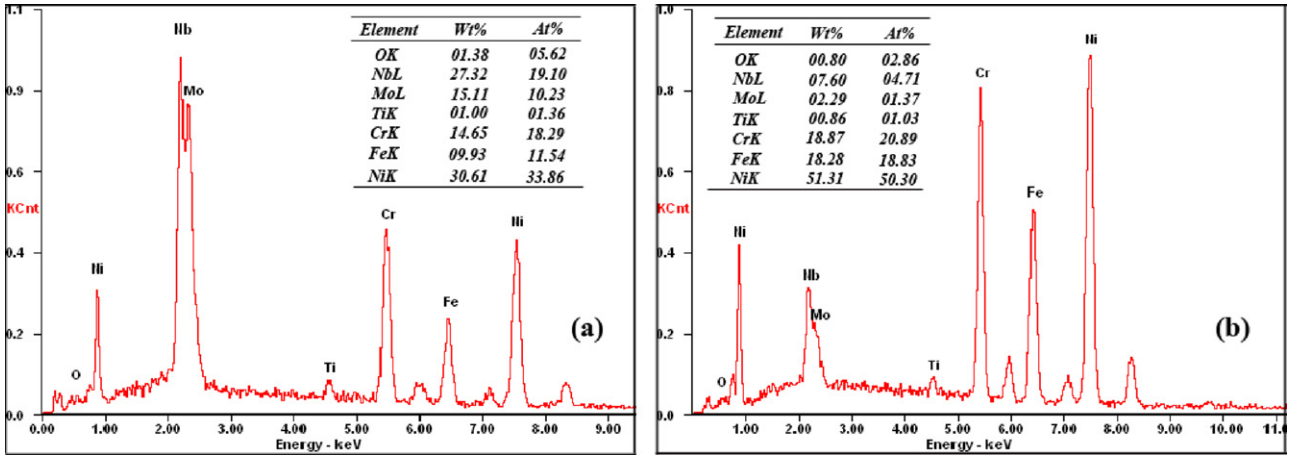

Fig. 7. EDS analysis results of the position P1, (a) and P2, (b) shown in Fig. 6 (b).

treated) samples, respectively. The microhardness of all samples shows directional independent though measurements along long distances (1.3–2.4 mm) have been conducted. There is no large microhardness fluctuation in *x*, *y* or 45° direction on both sections for all tested samples when measurement error is considered. Obviously, the interfaces of overlapping melted tracks and neighbor layers, which are often thought as metallurgical weaknesses, have no effect on the microhardness of samples by SLM and SLM + HT. It is also shown that the average microhardness (365 Hv) of SLMed samples is lower than that of the ordinary smelted IN718 followed by heat treatment (383 Hv). Obviously, though the grain refinement caused by laser rapid heating and cooling is helpful to the hardness of SLMed samples, heat treatment is still necessary to improve the hardness further. After solution and age-hardening treatment, the average microhardness increases remarkably to 470 Hv and is much higher than that of the ordinary smelted IN718 sample. The precipitation strengthening of γ' and γ'' to γ matrix and the intercrystalline strengthening of needle-like δ phase to grain boundaries are the main contributions for IN718 samples to their high microhardness without weakness. Furthermore, the effect of

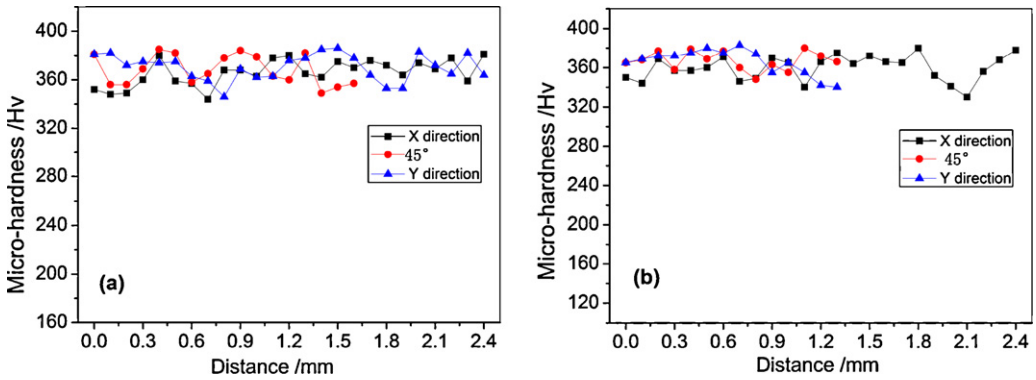

Fig. 8. Microhardness of SLMed IN718 samples on cross section (a) and vertical section (b).

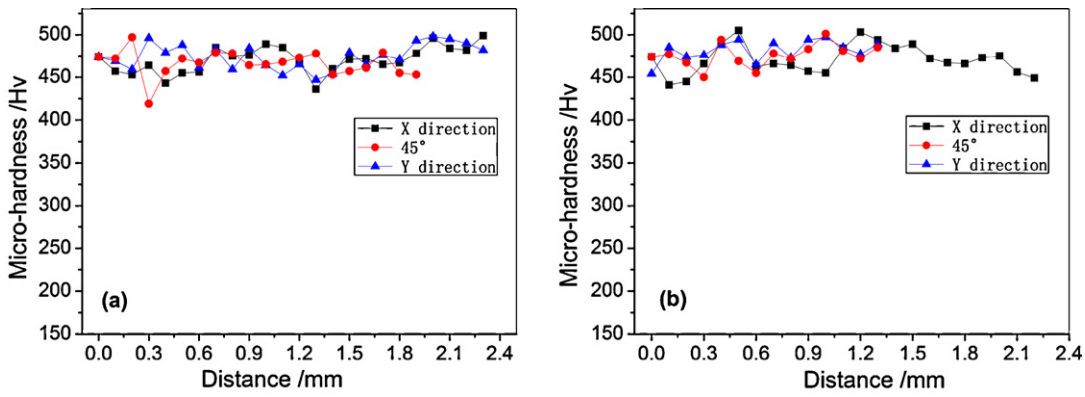

Fig. 9. Microhardness of SLM + HTed IN718 samples on cross section (a) and vertical section (b).

grain refinement on microhardness should not be ignored because the grain sizes are smaller than those obtained by conventional metallurgical methods though undergoing a post-heat treatment. Therefore, this higher microhardness is due to the combined effect of grain refinement and formation of precipitates by the post-heat treatment.

3.2.2. Tensile properties

The tensile properties of IN718 in as-deposited and heat-treated state at room temperature are presented in Table 3. For comparison, the tensile properties of the wrought IN718 are also included. Tensile strengths (ultimate strength (UTS) and yield strength ($\sigma_{0.2}$)) of the SLMed samples are inferior to those of the typical wrought IN718 alloy though their ductility is much higher. After heat treatment, the tensile strengths and ductility of the SLM + HTed IN718 at room temperature are comparative with those of the wrought IN718. Therefore, the tensile properties of the SLM + HTed IN718 are excellent enough to meet the needs of applications.

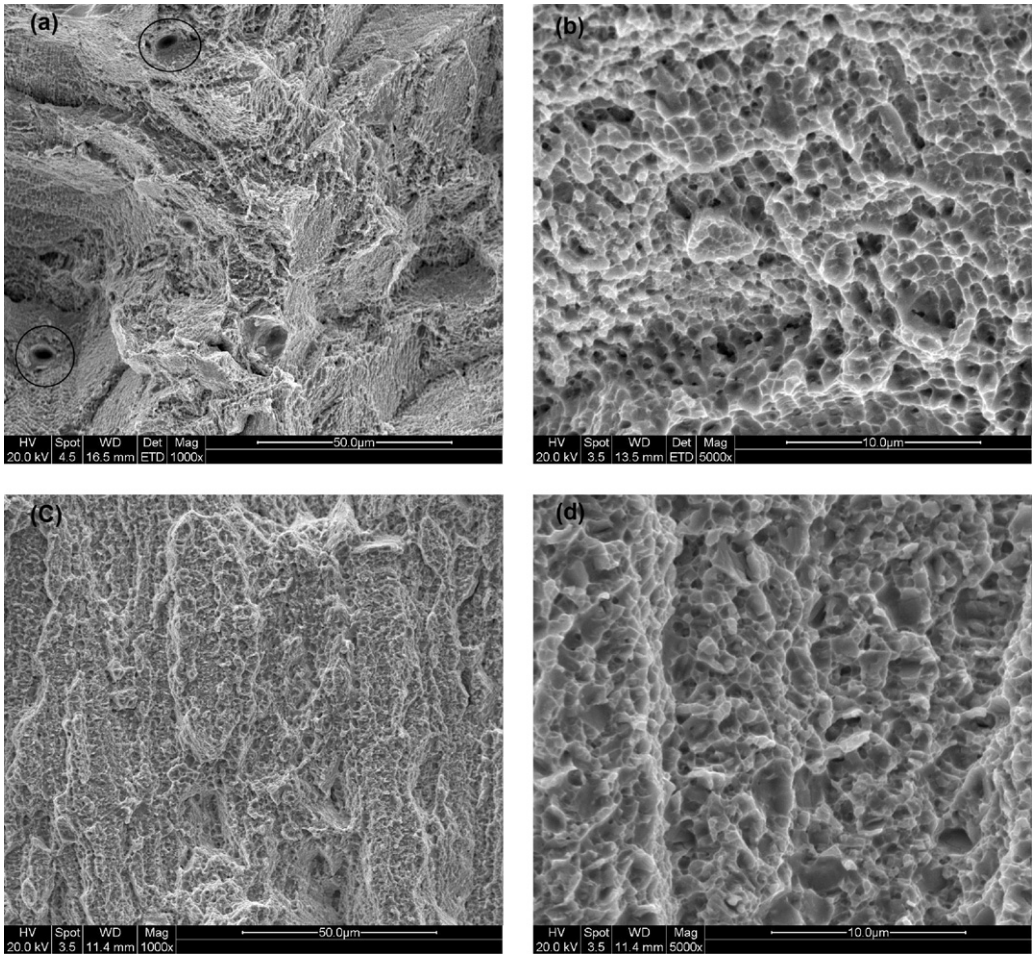

Fig. 10. Fractographs of IN718 at different states and room temperature. (a) SLMed samples at a low magnification, (b) SLMed samples at a high magnification, (c) SLM + HTed samples at a low magnification, and (d) SLM + HTed samples at a high magnification.

Table 3
Tensile test results for IN718 at different states.

Sample state	$\sigma_{0.2}$ (MPa)	UTS (MPa)	EL (%)	E (GPa)	Temperature
SLMed	889–907	1137–1148	19.2–25.9	204	RT
SLMed + HTed	1102–1161	1280–1358	10–22	201	RT
Wrought IN718 (AMS) [23]	1030–1167	1275–1400	12–21	208	RT

In order to investigate the fracture mechanism further, fracture surfaces of the tensile samples at different states are shown in Fig. 10. All the tensile samples exhibit the feature of ductile fracture for bestrewing dimples on the whole fracture surfaces. For the SLMed IN718 samples, the grain size is very small (shown in Fig. 5) because of the non-equilibrium melting and solidification caused by laser. Ordinarily, the tensile strengths and ductility should be improved more according to the Hall–Petch formula. But in Fig. 10(a), some micron-sized pores are observed in the SLMed samples, as pointed out by the circles. In general, the micro-pores not only reduce the stressed area but also damage the structural consistency in the as-deposited metal. The micro-pore plays a role as the crack initiator. During the tensile test, the micro-cracks usually initiate from these weakest positions due to the stress concentration, and then propagate to speed up the fracture. Therefore, compared with the other sample, shallow dimples with the smallest average size are formed (Fig. 10(b)), which leads to the inferior tensile strengths of the SLMed samples to those of the wrought IN718.

In Fig. 10(c) and (d), it can be seen that the dimples increase a little in size but become deeper than those in the as-deposited state owing to the precipitation strengthening after heat treatment. On the other hand, no micro-pores or other defects are found on the fracture surfaces. And thus, mechanical properties comparative with the wrought IN718 are obtained for SLM + HTed samples at room temperature.

In this study, formation features of SLM and heat treatment should be key factors to assure excellent mechanical properties of IN718. The fabrication process of parts by SLM is a powder metallurgical process based on continuous melting pools. These melting pools are in the class of micron-size due to micron-sizes of laser spot and powder layer thickness, which results in an average microdomain metallurgical quality without obvious defects. In addition, every metal powder layer with almost the same thickness is pre-deposited during SLM process. Melting pools induced by the scanning laser are basically equal in size and shape, which is benefit for the metallurgical uniformity of the whole part. Especially, the grains are very small due to a very high cooling rate induced by high laser energy density, which is also helpful to improve the mechanical properties of the fabricated IN718 parts. After ordinary solution and aging heat treatment, the mechanical properties of IN718 are developed completely by precipitation and grain boundary strengthening. Thus, good metallurgical microstructure, minimal defects and fine grains caused by SLM, as well as suitable heat treatment can assure excellent mechanical properties of IN718.

4. Summary

Selective laser melting of IN718 and post-heat treatment have been carried out to reveal the microstructure and mechanical properties. The microhardness of all samples shows directional independent. There is no large microhardness fluctuation in x, y or 45° direction on both sections for all tested samples. The average microhardness of the SLMed and SLM + HTed samples are 365 Hv and 470 Hv, respectively. After heat treatment, the tensile strengths and ductility of the SLM + HTed IN718 at room temperature are comparative with those of the wrought IN718. Good metallurgical bonding with minimal defects, grain refinement caused by laser rapid heating and cooling, and heat treatment are key factors to assure excellent mechanical properties of IN718.

Acknowledgement

This work is supported by the National Natural Science Foundation of China through Program nos. 50905068 and 51075164.

References

[1] H.Y. Zhang, S.H. Zhang, M. Cheng, Z.X. Li, Materials Characterization 61 (2010) 49–53.
[2] M. Anderson, R. Patwa, Y.C. Shin, International Journal of Machine Tools & Manufacture 46 (2006) 1879–1891.
[3] K.H. Song, K. Nakata, Journal of Alloys and Compounds 505 (2010) 144–150.
[4] H. Attia, S. Tavakoli, R. Vargas, V. Thomson, C.I.R.P. Annals, Manufacturing Technology 59 (2010) 83–88.
[5] J.P. Costes, Y. Guillet, G. Poulachon, M. Dessoly, International Journal of Machine Tools & Manufacture 47 (2007) 1081–1087.
[6] Z.Y. Wang, K.P. Rajurkar, J. Fan, S. Lei, Y.C. Shin, G. Petrescu, International Journal of Machine Tools & Manufacture 43 (2003) 1391–1396.
[7] A. Mugarra, K. Ostolaza, J.L. Alcaraz, Journal of Materials Processing Technology 125–126 (2005) 549–554.
[8] K. Osakada, M. Shiomi, International Journal of Machine Tools & Manufacture 46 (2006) 1188–1193.
[9] K.A. Mumtaz, N. Hopkinson, Journal of Materials Processing Technology 210 (2010) 279–287.
[10] M. Wong, I. Owen, C.J. Sutcliffe, A. Puri, International Journal of Heat and Mass Transfer 52 (2009) 281–288.
[11] D. Gu, Y. Shen, G. Meng, Materials Letters 63 (2009) 2536–2538.
[12] D. Buchbinder, H. Schleifenbaum, S. Heidrich, W. Meiners, J. Bültmann, Physics Procedia 12 (2011) 271–278.
[13] L. Jinhui, L. Ruidi, Z. Wenxian, F. Liding, Y. Huashan, Materials Science and Technology 26 (2010) 1259–1264.
[14] I. Yadroitsev, L. Thivillon, Ph. Bertrand, I. Smurov, Applied Surface Science 254 (2007) 980–983.
[15] P.L. Blackwell, Journal of Materials Processing Technology 170 (2005) 240–246.
[16] X. Zhao, J. Chen, X. Lin, W. Huang, Materials Science and Engineering A 478 (2008) 119–124.
[17] D. Clark, M.R. Bache, M.T. Whittaker, Journal of Materials Processing Technology 203 (2008) 439–448.
[18] G.D. Janaki Ram, A. Venugopal Reddy, K. Prasad Rao, G.M. Reddy, J.K. Sarin Sundar, Journal of Materials Processing Technology 167 (2005) 73–82.
[19] M.J. Cieslak, G.A. Knorovsky, T.J. Headley, A.D. Rimig Jr., The Minerals, Metals & Materials Society (1989) 59.
[20] J.N. DuPont, C.V. Robino, A.R. Marder, Welding Journal 77 (1998) 417s.
[21] A. Thomas, M. El-Wahabi, J.M. Cabrera, J.M. Prado, Journal of Materials Processing Technology 177 (2006) 469–472.
[22] L. Liu, C. Zhai, C. Lu, W. Ding, A. Hirose, K.F. Kobayashi, Corrosion Science 47 (2005) 355–367.
[23] G. Appa Rao, M. Srinivas, D.S. Sarma, Materials Science and Engineering A 383 (2004) 201–212.